Immobilizing Highly Catalytically Active Noble Metal Nanoparticles on Reduced Graphene Oxide: A Non-Noble Metal Sacrificial Approach

ARTICLE *in* JOURNAL OF THE AMERICAN CHEMICAL SOCIETY · JANUARY 2015

Impact Factor: 12.11 · DOI: 10.1021/ja511511q

4 AUTHORS, INCLUDING:

Qilong Zhu
National Institute of Advanced Industrial Sci…
43 PUBLICATIONS **740** CITATIONS
SEE PROFILE

Qiang xu
Hefei Union University
342 PUBLICATIONS **12,063** CITATIONS
SEE PROFILE

JACS
JOURNAL OF THE AMERICAN CHEMICAL SOCIETY
Communication
pubs.acs.org/JACS

Immobilizing Highly Catalytically Active Noble Metal Nanoparticles on Reduced Graphene Oxide: A Non-Noble Metal Sacrificial Approach

Yao Chen,[†] Qi-Long Zhu,[†] Nobuko Tsumori,[†,‡] and Qiang Xu*[,†]

[†]National Institute of Advanced Industrial Science and Technology (AIST), Ikeda, Osaka 563-8577, Japan
[‡]Toyama National College of Technology, 13, Hongo-machi, Toyama, 939-8630, Japan

Supporting Information

ABSTRACT: In this work, we have developed a non-noble metal sacrificial approach for the first time to successfully immobilize highly dispersed AgPd nanoparticles on reduced graphene oxide (RGO). The $Co_3(BO_3)_2$ co-precipitated with AgPd nanoparticles and subsequently sacrificed by acid etching effectively prevents the primary AgPd particles from aggregation. The resulted ultrafine AgPd nanoparticles exhibit the highest activity (turnover frequency, 2739 h^{-1} at 323 K) among all the heterogeneous catalysts for the dehydrogenation of formic acid to generate hydrogen without CO impurity. The sacrificial approach opens up a new avenue for the development of high-performance metal nanocatalysts.

Supported noble metal nanoparticles (NPs) have attracted great attention in catalysis due to their high activity in chemical reactions. Surface atoms often function as active sites, and thus the control of NP size can tailor the catalytic activity. Unfortunately, primary particles have high surface energies, rendering severe Oswald ripening or grain growth during the synthesis.[1] An efficient approach is to immobilize the NPs on special supports.[2] Among all the available support materials, reduced graphene oxide (RGO) consisting of chemically converted monolayer carbon atoms has emerged as one of the most promising supports for catalysts because the unique advantage of hydrophilicity and large specific surface area of its precursor, graphene oxide (GO), makes it possible to anchor well-dispersed metal NPs in the solution-based controlled reduction.[3] However, it is still a major obstacle to obtain monodispersed metal particles with very small sizes on unfunctionalized RGO, where the aggregation of NPs cannot be perfectly overcome.[4] Hence, immobilizing highly dispersed noble metal NPs with high catalytic activity on RGO remains a critical challenge in the heterogeneous catalysis.

On the other hand, formic acid (FA) has been proposed as a suitable liquid carrier for hydrogen,[5] which can be formed by a biomass processing[6] and reduction of carbon dioxide.[7] Hydrogen generation from FA holds great potential for application to hydrogen powered fuel cells (FCs),[8] and hence downsized metal NPs as high-performance nanocatalysts are highly desirable for this reaction.[9] Herein, for the first time, we report the immobilization of ultrafine AgPd NPs on RGO by a new non-noble metal sacrificial approach (NNMSA), in which a cobalt compound co-precipitated during the reduction of precursors and subsequently sacrificed by acid etching prevents the noble metal NPs from aggregation. The resulted catalyst exhibits the highest activity for the dehydrogenation of formic acid in the heterogeneous catalytic system.

Cobalt was chosen as the sacrificial agent for the NNMSA. The reaction between $Co(CH_3COOH)_2$ and $NaBH_4$ in a molar ratio of 1:3.7 under an ambient condition for 2 h results in the formation of a black precipitation, which exhibits very broad X-ray diffractions (XRD) (Figure 1a), characteristic of an amorphous phase. The sample crystallizes by annealing in Ar atmosphere at 823 K for 3 h, displaying the XRD peaks (Figure 1b) corresponding to $Co_3(BO_3)_2$ (JCPDS: 25-0102, Figure 1c).[10] The precipitation $Co_3(BO_3)_2$ can be readily dissolved in H_3PO_4 (Figure S1). The reaction between $NaBH_4$ and the mixed solution of $Co(CH_3COOH)_2$, $AgNO_3$, and K_2PdCl_4 in a molar ratio of 6:0.1:0.9 also produces a black precipitation

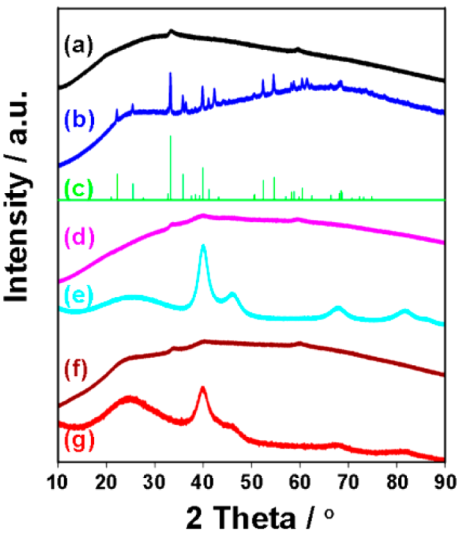

Figure 1. XRD patterns of the precipitations of the reaction between $Co(CH_3COOH)_2$ and $NaBH_4$ (a) before and (b) after annealing (823 K, 3 h, Ar), (c) JCPDS: 25-0102 ($Co_3(BO_3)_2$), (d) $Co_6Ag_{0.1}Pd_{0.9}$, (e) $(Co_6)Ag_{0.1}Pd_{0.9}$, (f) $Co_6Ag_{0.1}Pd_{0.9}$/RGO, and (g) $(Co_6)Ag_{0.1}Pd_{0.9}$/RGO.

Received: November 9, 2014

DOI: 10.1021/ja511511q
J. Am. Chem. Soc. XXXX, XXX, XXX−XXX

$Co_6Ag_{0.1}Pd_{0.9}$, giving an additional XRD peak at 39.9° for Pd (Figure 1d). Etching $Co_6Ag_{0.1}Pd_{0.9}$ with H_3PO_4 (2 h, room temperature) gives the sample $(Co_6)Ag_{0.1}Pd_{0.9}$, for which the broad XRD band due to $Co_3(BO_3)_2$ disappears while the characteristic Pd peaks are clearly observed (Figure 1e). In the presence of GO, the reaction between $NaBH_4$ and the mixed solution of $Co(CH_3COOH)_2$, $AgNO_3$, and K_2PdCl_4 in the same molar ratio (6:0.1:0.9) yields $Co_6Ag_{0.1}Pd_{0.9}$/RGO, which is followed by the H_3PO_4 etching to form $(Co_6)Ag_{0.1}Pd_{0.9}$/RGO. Both of $Co_6Ag_{0.1}Pd_{0.9}$/RGO and $(Co_6)Ag_{0.1}Pd_{0.9}$/RGO exhibit another broad XRD shoulder at 24° arising from RGO (Figure 1 f and g).[11]

The inductively coupled plasma optical emission spectroscopic analysis reveals that the molor ratio of Co:Ag:Pd in $(Co_6)Ag_{0.1}Pd_{0.9}$/RGO is 0.08:0.1:0.9, indicating that almost all the co-precipitated $Co_3(BO_3)_2$ can be removed by H_3PO_4. In the X-ray photoelectron spectroscopic (XPS) measurements, no Co 2p signals are observed for $(Co_6)Ag_{0.1}Pd_{0.9}$/RGO before and after Ar sputtering (Figure S2a). The Ag 3d and Pd 3d spectra reveal that $(Co_6)Ag_{0.1}Pd_{0.9}$/RGO is composed of metallic Ag and Pd covered by a thin oxidized layer[12] which can be easily removed by Ar sputtering (Figure S2b,c).

The morphologies of $Ag_{0.1}Pd_{0.9}$/RGO, $Co_6Ag_{0.1}Pd_{0.9}$/RGO and $(Co_6)Ag_{0.1}Pd_{0.9}$/RGO are investigated by transmission electron microscopy (TEM). $Ag_{0.1}Pd_{0.9}$/RGO exhibits severe aggregation of primary AgPd particles on RGO (Figure 2a).

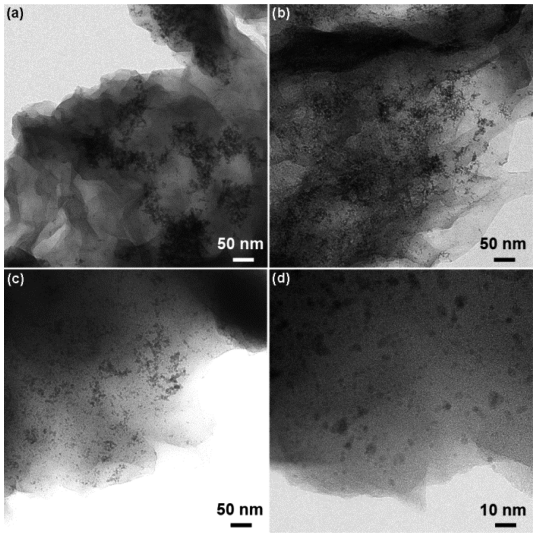

Figure 2. TEM images of (a) $Ag_{0.1}Pd_{0.9}$/RGO, (b) $Co_6Ag_{0.1}Pd_{0.9}$/RGO, and (c, d) $(Co_6)Ag_{0.1}Pd_{0.9}$/RGO.

More severe aggregation is observed for $Co_6Ag_{0.1}Pd_{0.9}$/RGO in Figures 2b and S3a. In contrast, $(Co_6)Ag_{0.1}Pd_{0.9}$/RGO shows highly dispersed NPs (2−4.5 nm) on RGO in Figures 2c,d and S3b. Combining with the XRD and ICP results, it can be concluded that the well-dispersed AgPd NPs are immobilized on RGO by NNMSA, illustrating that the sacrificial $Co_3(BO_3)_2$ prevents the primary AgPd particles from aggregation as shown in Scheme 1.

Figure 3 shows the nitrogen sorption isotherms of $Ag_{0.1}Pd_{0.9}$/RGO, $Co_6Ag_{0.1}Pd_{0.9}$/RGO, and $(Co_6)Ag_{0.1}Pd_{0.9}$/RGO. When AgPd NPs are loaded on RGO by direct deposition, the restacking of RGO is partially avoided. As a result, $Ag_{0.1}Pd_{0.9}$/RGO yields a type-IV curve with a hysteresis loop and a Brunauer−Emmett−Teller specific surface area of 183 $m^2\ g^{-1}$,

Scheme 1. Schematic Illustration of Immobilization of AgPd NPs on RGO by (a) direct deposition and (b) NNMSA

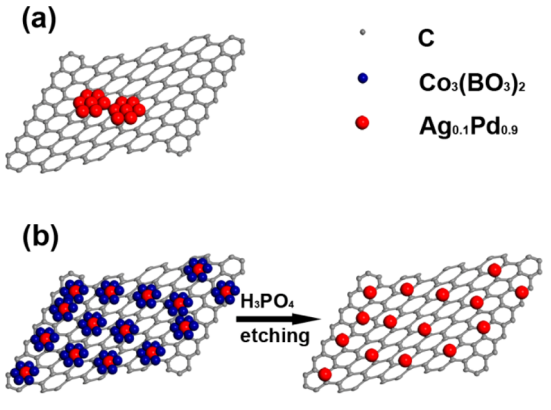

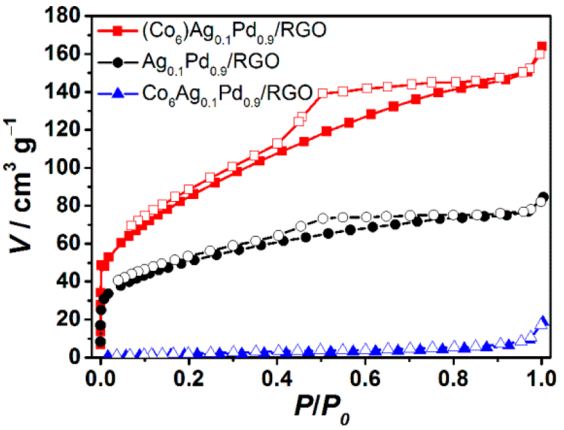

Figure 3. Nitrogen adsorption−desorption isotherms of $Ag_{0.1}Pd_{0.9}$/RGO, $Co_6Ag_{0.1}Pd_{0.9}$/RGO, and $(Co_6)Ag_{0.1}Pd_{0.9}$/RGO at 77 K.

indicative of mesopores between the RGO layers. $Co_6Ag_{0.1}Pd_{0.9}$/RGO shows a very low N_2 uptake with a specific surface area as low as 6 $m^2\ g^{-1}$, implying that the surface of separated RGO is completely occupied by a large amount of $Co_3(BO_3)_2$ with AgPd, which is consistent with the TEM observations. It is worth noting that a drastically increased N_2 uptake is observed for $(Co_6)Ag_{0.1}Pd_{0.9}$/RGO (310 $m^2\ g^{-1}$), illustrating that the elimination of $Co_3(BO_3)_2$ by the H_3PO_4 etching endows $(Co_6)Ag_{0.1}Pd_{0.9}$/RGO with high porosity, which would facilitate the diffusion of reactants to the metal NPs in catalysis.

Dehydrogenation of FA was selected as a probe reaction to investigate the catalytic performance of highly dispersed AgPd NPs on RGO. A series of $(Co_x)Ag_yPdy_{1-y}$/RGO catalysts (x represents the molar ratio of Co/(Ag + Pd) and y is the molar percentage of Ag in AgPd) are tested for hydrogen generation from FA in a FA−sodium formate (SF) system. At y = 0.1, the catalytic activity for the dehydrogenation of FA increases with increasing the amount of sacrificial $Co_3(BO_3)_2$ until x reaches 6 (Figures 4 and S4), illuminating that the non-noble metal sacrifical agent plays a decisive role in giving rise to high catalytic activity by decreasing the size of AgPd NPs. It is found that the molar ratio of SF to FA has an obvious effect on the performance of the $(Co_6)Ag_{0.1}Pd_{0.9}$/RGO catalyst. The activity of the catalyst for decomposition of FA increases with the molar ratio of SF to FA until the value reaches 2.5, after which further increase in the ratio of SF to FA does not give more positive effect on the decomposition of FA (Figure S5). The

DOI: 10.1021/ja511511q
J. Am. Chem. Soc. XXXX, XXX, XXX−XXX

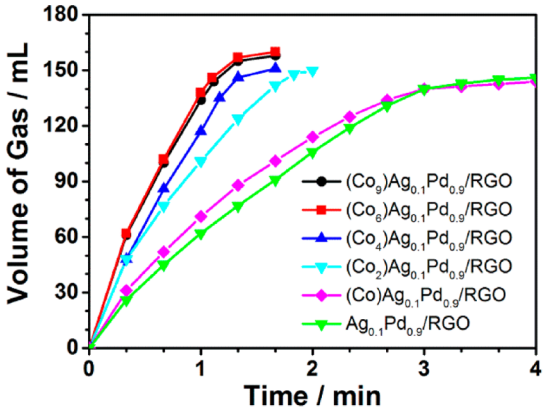

Figure 4. Volume of the generated gas (CO_2 + H_2) versus time for the dehydrogenation of FA over $(Co_x)Ag_{0.1}Pd_{0.9}$/RGO at 323 K (n_{AgPd}/n_{FA} = 0.02, n_{SF}/n_{FA} = 2.5).

decomposition of FA catalyzed by $(Co_6)Ag_{0.1}Pd_{0.9}$/RGO (n_{AgPd}/n_{FA} = 0.02, n_{SF}/n_{FA} = 2.5) is completed within 1.1 min with the generation of 146 mL gas (H_2 + CO_2). Gas chromatography measurements demonstrate that no CO can be detected from the evolved gas (H_2 + CO_2) at the level of 1 ppm (Figure S6). It is noted that the activity of (Co_6)-$Ag_{0.1}Pd_{0.9}$/RGO is much higher than that of (Co_6)Pd/RGO though monometallic Ag NPs on RGO is inactive for this reaction (Figure S7), indicating that Ag is an excellent promoter for Pd-catalyzed FA decomposition.[13] Additionally, both $(Co_6)Ag_{0.1}Pd_{0.9}$/RGO and $Ag_{0.1}Pd_{0.9}$/RGO show much better catalytic properties than the support-free $(Co_6)Ag_{0.1}Pd_{0.9}$ and $Ag_{0.1}Pd_{0.9}$ catalysts (Figure S8), suggesting that RGO as a support to immobilize the metal NPs is essential and effective for avoiding their aggregation. $(Co_6)Ag_{0.1}Pd_{0.9}$/RGO gives an average TOF of 2756 ± 180 h^{-1} at 323 K based on a full conversion of FA catalyzed by AgPd (Figure S4a), indicating that $(Co_6)Ag_{0.1}Pd_{0.9}$/RGO is the most active catalyst as the highest TOF record (2623 h^{-1}) was reported with the Pd/MSC-30 catalyst for the heterogeneous dehydrogenation of formic acid at 323 K.[14] It is worth noting that TOF of $(Co_6)Ag_{0.1}Pd_{0.9}$/RGO at 298 K (453 h^{-1}) is lower than that of Pd/MSC-30 (750 h^{-1}), opposite to the results at 323 K, for which the higher apparent activation energy of $(Co_6)Ag_{0.1}Pd_{0.9}$/RGO (43.1 kJ mol^{-1}) than that of Pd/MSC-30 (38.6 kJ mol^{-1})[14] accounts (Figure 5). For the durability test, the $(Co_6)Ag_{0.1}Pd_{0.9}$/RGO catalyst was recycled by washing with water after each cycle, of which the activity kept almost unchanged under the same reaction condition over 5 cycles (Figure S9), in agreement with the retained particle size of AgPd on RGO (Figure S10). The strong anchoring effect between the AgPd NPs and the RGO surface in (Co_6)-$Ag_{0.1}Pd_{0.9}$/RGO makes NNMSA an efficient approach toward the development of high-performance heterogeneous metal nanocatalysts.

In summary, we have developed a NNMSA, in which $Co_3(BO_3)_2$ co-precipitated with AgPd NPs and subsequently sacrificed by acid etching plays an important role in immobilizing highly dispersed AgPd NPs on RGO. The particle size of AgPd in $(Co_6)Ag_{0.1}Pd_{0.9}$/RGO prepared by NNMSA is much smaller than that in $Ag_{0.1}Pd_{0.9}$/RGO prepared by the direct deposition method. The $(Co_6)Ag_{0.1}Pd_{0.9}$/RGO catalyst shows much higher activity than $Ag_{0.1}Pd_{0.9}$/RGO for the FA dehydrogenation. The present strategy opens up a new

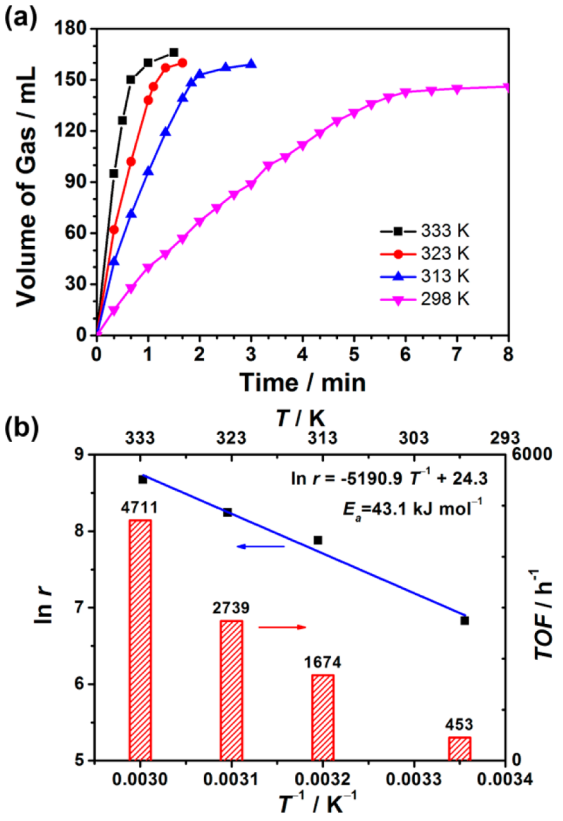

Figure 5. (a) Volume of the generated gas (CO_2 + H_2) versus time for the dehydrogenation of FA over $(Co_6)Ag_{0.1}Pd_{0.9}$/RGO at different temperatures, (b) Arrhenius plot and TOF values of the dehydrogenation of FA over $(Co_6)Ag_{0.1}Pd_{0.9}$/RGO (n_{AgPd}/n_{FA} = 0.02, n_{SF}/n_{FA} = 2.5).

avenue for the development of high-performance metal nanoparticle catalysts.

■ ASSOCIATED CONTENT

Ⓢ Supporting Information

Experimental details, additional material characterization and catalytic performance. This material is available free of charge via the Internet at http://pubs.acs.org.

■ AUTHOR INFORMATION

Corresponding Author

q.xu@aist.go.jp

Notes

The authors declare no competing financial interest.

■ ACKNOWLEDGMENTS

The authors thank the reviewers for valuable suggestions, Ms. Jun Li for XPS, and Dr. Takeyuki Uchida for TEM measurements and AIST and METI for financial support.

■ REFERENCES

(1) (a) Zaera, F. *Chem. Soc. Rev.* **2013**, *42*, 2746−2762. (b) Zhang, S.; Nguyen, L.; Zhu, Y.; Zhan, S.; Tsung, C.-K.; Tao, F. *Acc. Chem. Res.* **2013**, *46*, 1731−1739. (c) Thanh, N. T. K.; Maclean, N.; Mahiddine, S. *Chem. Rev.* **2014**, *114*, 7610−7630.

(2) (a) Li, P.-Z.; Aijaz, A.; Xu, Q. *Angew. Chem., Int. Ed.* **2012**, *51*, 6753−6756. (b) Aijaz, A.; Karkamkar, A.; Choi, Y. J.; Tsumori, N.; Rönnebro, E.; Autrey, T.; Shioyama, H.; Xu, Q. *J. Am. Chem. Soc.* **2012**, *134*, 13926−13929. (c) Yin, H.; Tang, H.; Wang, D.; Gao, Y.;

DOI: 10.1021/ja511511q
J. Am. Chem. Soc. XXXX, XXX, XXX−XXX

Tang, Z. *ACS Nano* **2012**, *6*, 8288−8297. (d) Kuo, C.-H.; Tang, Y.; Chou, L.-Y.; Sneed, B. T.; Brodsky, C. N.; Zhao, Z.; Tsung, C.-K. *J. Am. Chem. Soc.* **2012**, *134*, 14345−14348. (e) Guo, Z.; Xiao, C.; Maligal-Ganesh, R. V.; Zhou, L.; Goh, T. W.; Li, X.; Tesfagaber, D.; Thiel, A.; Huang, W. *ACS Catal.* **2014**, *4*, 1340−1348.

(3) (a) Tan, C.; Huang, X.; Zhang, H. *Mater. Today* **2013**, *16*, 29−36. (b) Liu, M.; Zhang, R.; Chen, W. *Chem. Rev.* **2014**, *114*, 5117−5160.

(4) (a) Guo, S.; Dong, S.; Wang, E. *ACS Nano* **2009**, *4*, 547−555. (b) Parvez, K.; Yang, S.; Hernandez, Y.; Winter, A.; Turchanin, A.; Feng, X.; Müllen, K. *ACS Nano* **2012**, *6*, 9541−9550. (c) Tiwari, J. N.; Nath, K.; Kumar, S.; Tiwari, R. N.; Kemp, K. C.; Le, N. H.; Youn, D. H.; Lee, J. S.; Kim, K. S. *Nat. Commun.* **2013**, *4*, 2221. (d) Shin, S. I.; Go, A.; Kim, I. Y.; Lee, J. M.; Lee, Y.; Hwang, S.-J. *Energy Environ. Sci.* **2013**, *6*, 608−617. (e) Shang, L.; Bian, T.; Zhang, B.; Zhang, D.; Wu, L.-Z.; Tung, C.-H.; Yin, Y.; Zhang, T. *Angew. Chem., Int. Ed.* **2014**, *53*, 250−254.

(5) (a) Fellay, C.; Dyson, P. J.; Laurenczy, G. *Angew. Chem., Int. Ed.* **2008**, *47*, 3966−3968. (b) Ojeda, M.; Iglesia, E. *Angew. Chem., Int. Ed.* **2009**, *48*, 4800−4803. (c) Boddien, A.; Mellmann, D.; Gärtner, F.; Jackstell, R.; Junge, H.; Dyson, P. J.; Laurenczy, G.; Ludwig, R.; Beller, M. *Science* **2011**, *333*, 1733−1736. (d) Yadav, M.; Singh, A. K.; Tsumori, N.; Xu, Q. *J. Mater. Chem.* **2012**, *22*, 19146−19150. (e) Martis, M.; Mori, K.; Fujiwara, K.; Ahn, W.-S.; Yamashita, H. *J. Phys. Chem. C* **2013**, *117*, 22805−22810. (f) Mori, K.; Dojo, M.; Yamashita, H. *ACS Catal.* **2013**, *3*, 1114−1119. (g) Jiang, K.; Xu, K.; Zou, S.; Cai, W.-B. *J. Am. Chem. Soc.* **2014**, *136*, 4861−4864. (h) Zhu, Q.-L.; Xu, Q. *Energy Environ. Sci.* **2015**, DOI: 10.1039/C4EE03690E.

(6) (a) Jin, F.; Yun, J.; Li, G.; Kishita, A.; Tohji, K.; Enomoto, H. *Green Chem.* **2008**, *10*, 612−615. (b) Wang, W.; Niu, M.; Hou, Y.; Wu, W.; Liu, Z.; Liu, Q.; Ren, S.; Marsh, K. N. *Green Chem.* **2014**, *16*, 2614−2618.

(7) (a) Grasemann, M.; Laurenczy, G. *Energy Environ. Sci.* **2012**, *5*, 8171−8181. (b) Hull, J. F.; Himeda, Y.; Wang, W.-H.; Hashiguchi, B.; Periana, R.; Szalda, D. J.; Muckerman, J. T.; Fujita, E. *Nat. Chem.* **2012**, *4*, 383−388. (c) Centi, G.; Quadrelli, E. A.; Perathoner, S. *Energy Environ. Sci.* **2013**, *6*, 1711−1731. (d) Moret, S.; Dyson, P. J.; Laurenczy, G. *Nat. Commun.* **2014**, *5*, 4017.

(8) (a) Boddien, A.; Loges, B.; Junge, H.; Beller, M. *ChemSusChem* **2008**, *1*, 751−758. (b) Boddien, A.; Federsel, C.; Sponholz, P.; Mellmann, D.; Jackstell, R.; Junge, H.; Laurenczy, G.; Beller, M. *Energy Environ. Sci.* **2012**, *5*, 8907−8911. (c) Yadav, M.; Xu, Q. *Energy Environ. Sci.* **2012**, *5*, 9698−9725.

(9) (a) Gu, X.; Lu, Z.-H.; Jiang, H.-L.; Akita, T.; Xu, Q. *J. Am. Chem. Soc.* **2011**, *133*, 11822−11825. (b) Bi, Q.-Y.; Du, X.-L.; Liu, Y.-M.; Cao, Y.; He, H.-Y.; Fan, K.-N. *J. Am. Chem. Soc.* **2012**, *134*, 8926−8933. (c) Wang, Z.-L.; Yan, J.-M.; Ping, Y.; Wang, H.-L.; Zheng, W.-T.; Jiang, Q. *Angew. Chem., Int. Ed.* **2013**, *52*, 4406−4409. (d) Hu, C.; Pulleri, J. K.; Ting, S.-W.; Chan, K.-Y. *Int. J. Hydrogen Energy* **2014**, *39*, 381−390.

(10) Glavee, G. N.; Klabunde, K. J.; Sorensen, C. M.; Hadjapanayis, G. C. *Langmuir* **1992**, *8*, 771−773.

(11) Chen, Y.; Zhang, X.; Zhang, D.; Yu, P.; Ma, Y. *Carbon* **2011**, *49*, 573−580.

(12) Chen, L.; Yelon, A.; Sacher, E. *J. Phys. Chem. C* **2011**, *115*, 7896−7905.

(13) (a) Tedsree, K.; Li, T.; Jones, S.; Chan, C. W. A.; Yu, K. M. K.; Bagot, P. A. J.; Marquis, E. A.; Smith, G. D. W.; Tsang, S. C. E. *Nat. Nanotechnol.* **2011**, *6*, 302−307. (b) Zhang, S.; Metin, Ö.; Su, D.; Sun, S. *Angew. Chem., Int. Ed.* **2013**, *52*, 3681−3684. (c) Dai, H.; Cao, N.; Yang, L.; Su, J.; Luo, W.; Cheng, G. *J. Mater. Chem. A* **2014**, *2*, 11060−11064.

(14) Zhu, Q.-L.; Tsumori, N.; Xu, Q. *Chem. Sci.* **2014**, *5*, 195−199.

DOI: 10.1021/ja511511q
J. Am. Chem. Soc. XXXX, XXX, XXX−XXX